Hindawi
Journal of Electrical and Computer Engineering
Volume 2018, Article ID 8260479, 16 pages
https://doi.org/10.1155/2018/8260479

Research Article

Reliability Analysis of Network Real-Time Kinematic

Mohammed Ouassou,[1] **Bent Natvig**,[2] **Anna B. O. Jensen**,[3] **and Jørund I. Gåsemyr**[2]

[1]*Norwegian Mapping Authority, Geodetic Institute, 3511 Hønefoss, Norway*
[2]*UiO, Department of Mathematics, Norway*
[3]*KTH Royal Institute of Technology, 10044 Stockholm, Sweden*

Correspondence should be addressed to Mohammed Ouassou; mohammed.ouassou@statkart.no

Received 30 November 2017; Accepted 27 March 2018; Published 6 June 2018

Academic Editor: Sandro M. Radicella

Copyright © 2018 Mohammed Ouassou et al. This is an open access article distributed under the Creative Commons Attribution License, which permits unrestricted use, distribution, and reproduction in any medium, provided the original work is properly cited.

The multistate reliability theory was applied to the network real-time kinematic (NRTK) data processing chain, where the qualities of the network corrections, baseline residuals, and the associated variance-covariance matrices are considered as the system state vectors. The state vectors have direct influence on the rover receiver position accuracy. The penalized honored stochastic averaged standard deviation (PHSASD) is used to map the NRTK sensitive data, represented by the states vectors to different levels of performance. The study shows that the improvement is possible by identification of critical components in the NRTK system and implementation of some parallelism that makes the system more robust.

1. Introduction

High accuracy positioning with GNSS is carried out using both code and carrier phase data from the GNSS satellites. To obtain position accuracies at the cm or mm level using carrier phase data, an important part of the data processing is to estimate the initial oscillator phase offset, the so-called ambiguity, for each receiver-satellite pair. Resolution of ambiguities requires that the influence of most errors sources in the positioning process is reduced to the cm-level, and high accuracy positioning is therefore often done in a relative mode where the position of a GNSS receiver located in an unknown position (the rover) is determined relative to one or more reference stations located in positions known on beforehand [1].

With relative carrier phase based GNSS positioning the effects of the distance-dependent error sources such as uncertainties in satellite positions and atmospheric effects on the satellite signals induced by the ionosphere and troposphere are reduced. Also the effects of satellite and receiver clock errors in the positioning process are reduced by relative positioning, and all this in combination makes it possible to resolve the ambiguities and thereafter obtain positions for the rover at the cm or mm level.

For high accuracy GNSS positioning in real time, the real time kinematic (RTK) technique has been developed. Traditionally this is based on a reference station transmitting data to the rover where the data is used in estimation of the position of the rover in a relative or differential mode [2].

Using a network of reference stations for RTK, the so-called NRTK technique, provides the opportunity for applying more advanced algorithms for estimation of the distance-dependent errors within the network and thereby possibilities for providing a more robust service. Such operational NRTK services exist in many regions and countries today and have become an indispensable tool in high accuracy navigation and surveying.

A brief description of the NRTK functionality is as follows: the first step is collection of raw observations from the network of reference stations, solving the ambiguities within the reference network, and generating error estimates. Then an interpolation/smoothing scheme is applied to generate the NRTK corrections for the user location. For information on how to avoid a loss of information under interpolation of NRTK data, the interested reader is referred to [3].

The NRTK corrections are then transmitted to rover receivers. Several NRTK techniques exist and the most

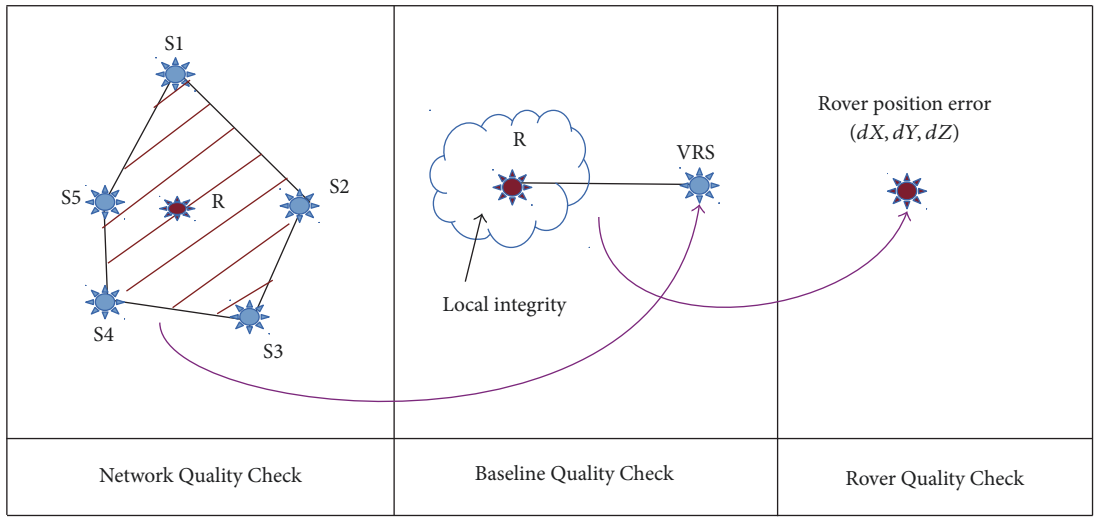

Figure 1: NRTK processing chain. The left panel shows NRTK module that produces the network corrections. The curved line indicates the output generated by the network module. Middle panel shows the local and the baseline processing module. Right panel shows the rover position solution module.

commonly used at present are, for instance, the Master Auxiliary Concept (MAC) [4, 5], the Virtual Reference Station (VRS) concept [6], and the FKP techniques [7], as well as the Network Adjustment (NetAdjust) concept developed by Raquet and Lachapelle [8, 9].

Multistate system reliability theory has been a research topic for many years, for instance, extension of the system from two-state to multistate reliability [10, 11] to compute the mean performance level at any given time t and stochastic evaluation and bound computation of multistate coherent systems [12], further, studies on application of reliability analysis to GNSS data processing [2], a comparative GNSS reliability analysis [13], reliability analysis under GNSS weak signals [14], accuracy and reliability of multi-GNSS real-time precise positioning [15], and robust reliability testing in case of signal degradation environment [16, 17].

In order to avoid confusion between the reliability theory definition used in different fields, we refer to the traditional reliability theory to the context of statistical testing based on the theory developed by Baarda [18], while component, system, binary, and multistate reliability terms will be used in case of component and system reliability computation.

Our aim is to provide the user in the field with continuously high quality corrections with the ability to identify the periods for which the reliability of the network RTK performance is reduced in terms of accuracy and availability. Therefore, solution quality indicators describing the reliability of the network RTK are needed to transfer the status of the network to the user in the field. Intensive research has been conducted recently in this field to derive these quality indicators and can be classified into two main classes; (i) spatially correlated (ionosphere, troposphere, and orbital) error indicators; (ii) residuals errors indicators. Most network RTK used quality indicators are residual integrity monitoring (RIM) and irregularity parameters (IP) quality indices [19], residual interpolation uncertainty (RIU) [20], geometry-based quality indicator (GBI) [21], and ionospheric index I95 [20]. An elegant presentation summarizing the network RTK quality indicators can be found in [22].

In order to apply reliability analysis to a NRTK system, the starting point is the decomposition of the block diagrams of NRTK processing chain into simple components and computation of the system reliability. Figure 1 shows three levels of data processing modules, the network, the baseline, and the rover receiver modules, where R denotes rover, S denotes reference station, and (dX, dY, dZ) denote errors in the position X, Y, Z coordinates, respectively. Based on these levels, we can build the reliability block diagrams for the NRTK processing chain and compute the reliability for the entire system.

The rest of the paper is organized as follows:

Section 2: brief introduction to component, system, and binary state reliability theory and deterministic and stochastic reliability.

Section 3: NRTK blocks diagram determination and module reliability computations.

Section 4: multistate reliability theory applied to NRTK processing chain.

Section 5: some test results.

Section 6: procedures used to validate the NRTK system reliability.

Section 7: discussions and conclusion.

Test data used in this investigation is described in Appendix A.

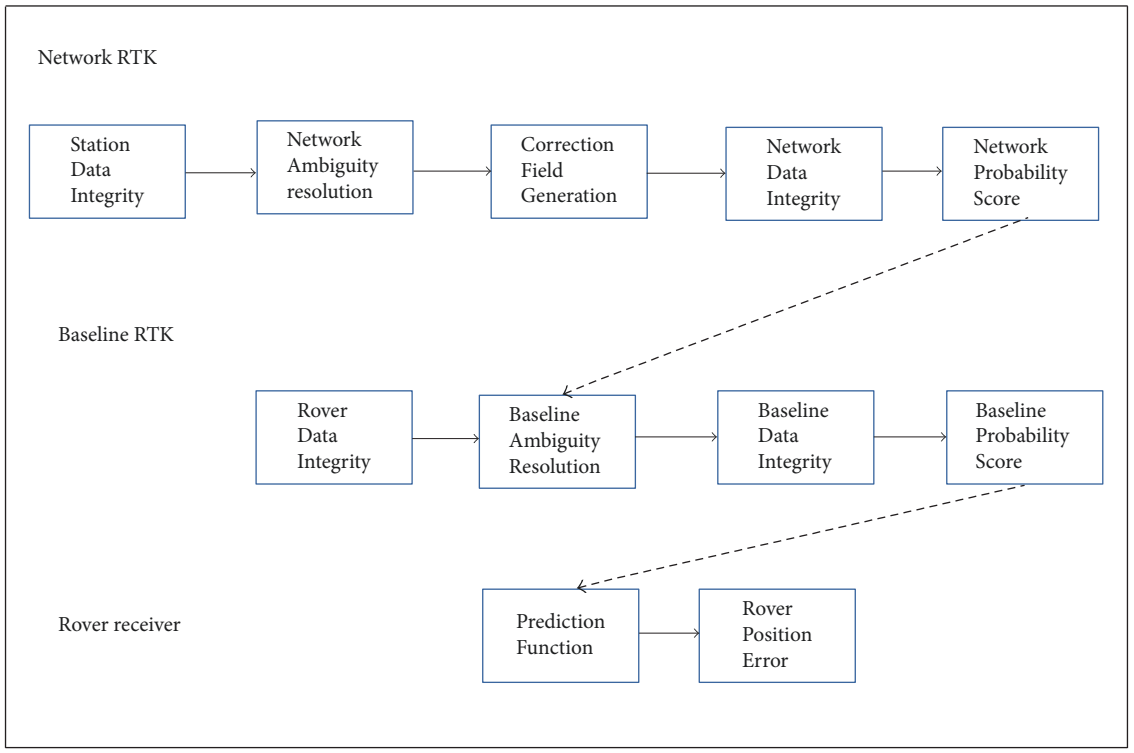

Figure 2: Network real-time kinematic processing chain main modules. Dotted lines describe the components dependency from different levels.

2. Reliability Analysis

The aim of this section is to introduce the basic of the component, system, and binary state reliability theory, including deterministic and stochastic reliability, followed by decomposing the block diagrams of the NRTK processing chain into simple components, and compute the entire system reliability. The description of the structural relationship between the components and the system must be defined. Figure 2 illustrates the concept and each main block will be treated separately in the coming sections.

2.1. Structure Functions. In order to construct the entire reliability block diagram of the NRTK data integrity, it is necessary to define the elementary building blocks as Bernoulli indicator function [23, pp. 28-29]. The function will signal if a unit or system is functioning or not.

A random variable X is said to be a Bernoulli random variable if its probability function is given by (1). The indicator and structure functions are given below by following the notation given by Natvig [24]:

$$X_i = \begin{cases} 1, & \text{success with probability } p, \\ 0, & \text{failure with probability } (1-p). \end{cases} \tag{1}$$

2.1.1. Bernoulli Indicator Function. Let x_i denote the indicator function of component, i. Then we have

$$x_i = \begin{cases} 1, & \text{if the } i\text{'th component is functioning,} \\ 0, & \text{otherwise.} \end{cases} \tag{2}$$

2.1.2. System Structure Function. Let the state vector $\mathbf{x} = (x_1, x_2, \ldots, x_n)$ give which components are functioning and which are not.

Let $\phi(\mathbf{x})$ denote the Bernoulli indicator of the state vector, $\mathbf{x}$. Then we have

$$\phi(\mathbf{x}) = \begin{cases} 1, & \text{if the system is functioning} \\ 0, & \text{otherwise} \end{cases} \tag{3}$$

$\phi(\mathbf{x})$ is the structure function of the system.

2.1.3. Series Structure Function. The series structure function $\phi_s(\mathbf{x})$ works *if and only if all components* of the state vector $\mathbf{x}$ are functioning. The series structure function $\phi_s(\mathbf{x})$ reads

$$\phi_s(\mathbf{x}) = \min(x_1, x_2, \ldots, x_n) = \prod_{i=1}^{n} x_i. \tag{4}$$

2.1.4. Parallel Structure Function. The parallel structure function $\phi_p(\mathbf{x})$ works *if and only if at least one* of the components of the state vector $\mathbf{x}$ is functioning. The parallel structure function $\phi_p(\mathbf{x})$ reads

$$\begin{aligned} \phi_p(\mathbf{x}) &= \max(x_1, x_2, \ldots, x_n) = 1 - \prod_{i=1}^{n} (1 - x_i) \\ &= \coprod_{i=1}^{n} x_i, \end{aligned} \tag{5}$$

where $\coprod$ is read "ip" and denotes the parallel coupling operator.

2.1.5. k-out-of-n Structure Function. A system composed of n components which is functioning *if and only if at least* k components are functioning is called a *k-out-of-n structure*

$$\phi_{k,n}(\mathbf{x}) = \begin{cases} 1, & \text{if } \sum_{i=1}^{n} x_i \geq k, \\ 0, & \text{otherwise.} \end{cases} \tag{6}$$

Note that the structure functions given by (4) and (5) are an *n-out-of-n structure* and an *1-out-of-n structure*, respectively. Other structure functions exist, for instance, the bridge Natvig [24, p. 12].

2.2. System Reliability Computation. The structure functions are defined; now is time to compute the system reliability. We move from the deterministic model to the stochastic one by introducing the random variables. Some notations are needed to represent the state vector, structure function, and the reliability. We follow the notations given by Hoyland and Rausand [25, Chaps. 3–5]. We denote the state variables of the n independent component at time t by

$$X_1(t), X_2(t), \ldots, X_n(t). \tag{7}$$

The corresponding state vector and the structure function are denoted, respectively, by

$$\begin{gathered} \mathbf{X}(t) = \left(X_1(t), X_2(t), \ldots, X_n(t)\right), \\ \phi(\mathbf{X}(t)). \end{gathered} \tag{8}$$

The probabilities of interest are presented by

$$\begin{aligned} P\left(\mathbf{X}_i(t) = 1\right) &= p_i(t) \quad \text{for } i = 1, 2, \ldots, n, \\ P\left(\phi(\mathbf{X}(t) = 1)\right) &= p_s(t), \end{aligned} \tag{9}$$

where $p_i(t)$ is the component reliability while $p_s(t)$ is the system reliability. Assuming that the components are independent, then the computation of the reliability of the state vector $\mathbf{X}(t)$ and the system $\phi(\mathbf{X}(t))$ at time t are defined as the expectation operator

$$\begin{aligned} \mathbb{E}\left(X_i(t)\right) &= 0 \cdot P\left(X_i(t) = 0\right) + 1 \cdot P\left(X_i(t) = 1\right) \\ &= p_i(t) \quad \text{for } i = 1, 2, \ldots, n. \end{aligned} \tag{10}$$

Let R denote the system reliability, then we have

$$\begin{aligned} \mathbb{E}\left(\phi(\mathbf{X}(t))\right) &= p_s(t) = R\left(p_1(t), p_2(t), \ldots, p_n(t)\right) \\ &= R(\mathbf{p}(t)). \end{aligned} \tag{11}$$

To avoid confusion, $p_i = P(X_i(t) = 1)$ is the probability of functioning of the ith component and referred to as the component reliability.

2.2.1. Reliability of Series Structures. The reliability function $R_s(\mathbf{p})$ of the series system of n independent components is given by the expression:

$$\begin{aligned} R_s(\mathbf{p}) &= P\left(\phi(\mathbf{X}(t) = 1)\right) \\ &= P\left\{X_i(t) = 1 \ \forall i = 1, 2, \ldots, n\right\} = \prod_{i=1}^{n} p_i(t). \end{aligned} \tag{12}$$

If all components have the same $p(t)$, (12) becomes $\{p(t)\}^n$. For $n = 5$ and $p = 0.99$, then the reliability $R_s(\mathbf{p}) = 0.951$.

An important remark is that the reliability of a series structure is at most as reliable as the least reliable component, that is, $R_s(\mathbf{p}) \leq \min_i(p_i(t))$.

2.2.2. Reliability of Parallel Structures. The reliability function $R_p(\mathbf{p})$ of the parallel system of n independent components is given by the expression:

$$\begin{aligned} R_p(\mathbf{p}) &= P\left(\phi(\mathbf{X}(t) = 1)\right) \\ &= P\left\{X_i(t) = 1 \text{ for some } i = 1, 2, \ldots, n\right\} \\ &= 1 - P\left\{X_i(t) = 0 \ \forall i = 1, 2, \ldots, n\right\} \\ &= 1 - \prod_{i=1}^{n} \left(1 - p_i(t)\right) \end{aligned} \tag{13}$$

If all components have the same $p(t)$, (13) becomes $1 - \{1 - p(t)\}^n$. For $n = 5$ and $p = 0.99$, then the reliability $R_p(\mathbf{p}) = 1$.

An important remark is that the reliability of a parallel structure is at least as reliable as the most reliable component, that is, $R(\mathbf{p}) \geq \max_i(p_i(t))$.

Details on how to compute the reliability of parallel structure in general are given in Appendix C.

2.2.3. Reliability of k-out-of-n Structures. The reliability function $R_{(k-n)}(\mathbf{p})$ of the k-out-of-n system of n independent components with equal probability $p_i(t) = p$ is given by the expression:

$$\begin{aligned} R_{(k-n)}(\mathbf{p}) &= P\left(\phi(\mathbf{X}(t) = 1)\right) = P\left\{\sum_{i=1}^{n} X_i(t) \geq k\right\} \\ &= \sum_{i=k}^{n} \binom{n}{i} \cdot p^i (1-p)^{n-i}. \end{aligned} \tag{14}$$

3. Reliability in the NRTK Processing Chain

The aim of this section is to determine the structure functions, NRTK module's reliability, and the corresponding block diagrams.

3.1. Considerations around NRTK Data Processing. Some considerations around the NRTK data integrity are introduced below as a background for the design process and to ease the discussions in the following sections. For more information on GNSS data processing, the reader is referred

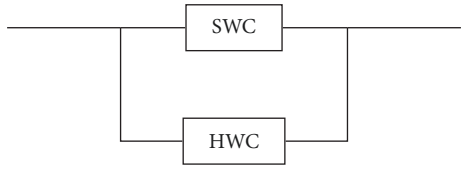

Figure 3: Main block diagram of module $M_{N,1}$.

to [1, 2, 26, 27]. The key to precise positioning is the correct ambiguity resolution and validation. With ambiguities resolved to wrong integer numbers, there will be offsets in the position solution, and with float ambiguities (ambiguities that are not fixed to integer values) the position solution is inaccurate and also very unstable and sensitive to changes in satellite geometry.

Good satellite-receiver geometry, as, for instance, expressed by the so-called DOP factor (dilution of precision), is important to perform successful ambiguity resolution and achieve centimeter level accuracy in real time.

Spatiotemporal models that describe well the variations of the spatially correlated errors in the corrections field are also an important key for reliable NRTK positioning.

Robust estimation algorithms to handle large data sets are also a key factor becoming more important in the future as observations from several GNSS systems to a larger degree will be combined in one processing loop. Today, most NRTK systems operate with data from the American GPS and the Russian GLONASS system. Including data from the European Galileo as well as the Chinese Beidou systems in NRTK operations will soon be the norm for most NRTK services. With satellites from more GNSS systems being available the satellite-receiver geometry on the rover side is improved. This is especially important when the user is operating in constricted environments such as narrow street canyons or forest areas.

3.2. NRTK Corrections Reliability Analysis. The main function of the NRTK is to provide the rover in the field with high quality corrections on an epoch-by-epoch basis.

From Figure 2, five modules $M_{N,i}$ are defined for the network and the reliability of each module will be evaluated. $M_{i,j}$ corresponds to level $i \in \{N, B, R\}$ and module $j \in \{1, 2, \ldots, 5\}$, where N stands for network, B for baseline, and R for rover receiver. For instance, the module $M_{N,1}$ corresponds to the first network module, the Station Data Integrity, as shown in Figure 2, and $M_{R,1}$ denotes the first of the rover modules, i.e., the Prediction Function as shown in Figure 2.

3.2.1. Reference Receivers Data Integrity. Generation of high quality raw observations at reference receivers requires reliable hardware (HWC) and software (SWC) components. Expensive hardware and sophisticated algorithms are keys to achieve this goal. Figure 3 shows the concept and each component will be treated separately in the next sections.

Let software and hardware components be represented by the modules $M_{N,1,X}$ and $M_{N,1,Y}$, respectively.

Software Component of Module $M_{N,1}$ Definition. SWC requires an ensemble of sequential checks on raw observations. This includes

(i) Let $x_{1,1}$ denote the satellite data integrity algorithm. This algorithm will discard the measurements from unhealthy satellite(s) or from satellite(s) for which we do not have the orbital data.

(ii) Let $x_{1,2}$ denote controlled cycle-slip algorithm. This task requires investigation of carrier phase discontinuities by examination of loss of lock (LLI) indicator and signal-to-noise ratio (SNR) flags.

(iii) Let $x_{1,3}$ denote uncontrolled cycle-slips in the observations. The algorithm uses the observation combinations for this purpose. The interested reader is referred to [27, pp. 95–101].

(iv) Let $x_{1,4}$ denote the reference receiver clock offset reset algorithm. Continual corrections are carried out to reduce the effect of the jump. The receiver clock offset (jump with ±1 ms) must be detected and corrected because they cause jump in carrier phase.

(v) Let $x_{1,5}$ denote outliers detection and repair algorithm.

(vi) Let $x_{1,6}$ denote the low elevation angle. Algorithm prunes satellite(s) based on their low elevation angle.

(vii) Let $x_{1,7}$ denote the minimum observations required to generate the corrections. At least 4 observation types are needed (L_1, L_2, P_1, and P_2). For more information about the observation types provided by satellites, the reader is referred to [28].

(viii) Let $x_{1,8}$ denote the reference receiver clock stability algorithm.

(ix) Let $x_{1,9}$ denote the multipath mitigation algorithm.

(x) Let $x_{1,10}$ denote the reweighting algorithm. All units are parallel coupled.

(1) Let $x_{[1,10,1]}$ denote a low elevation reweighting algorithm.

(2) Let $x_{[1,10,2]}$ denote a scintillation reweighting algorithm.

(3) Let $x_{[1,10,3]}$ denote a signal-to-noise reweighting algorithm.

Figure 5 shows the block diagram of the network reweighting algorithm component $x_{1,10}$.

Block Diagram and Reliability of Software Component. The structure function of the software component is well described by the 5-out-of-10 structure function. This means that the more algorithms check is, the more reliable raw observations become.

In order to produce reliable raw observations of high quality, it is necessary to perform at least five checks from a total of ten. With ten algorithms' check, we can generate high quality raw observations while five algorithms' check

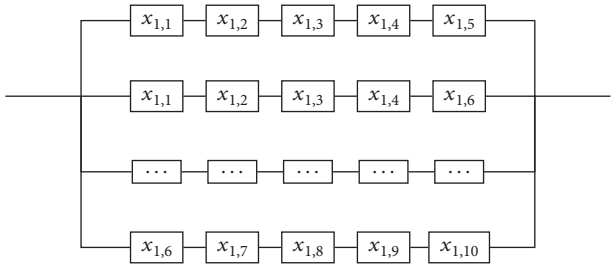

Figure 4: Block diagram of software component of network module $M_{N,1}$.

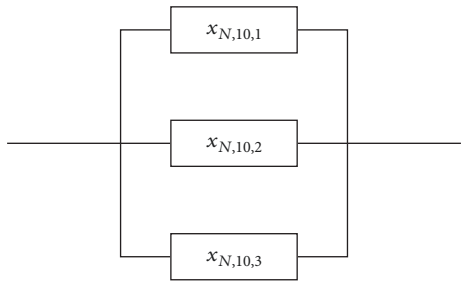

Figure 5: Block diagram of the network unit $x_{1,10}$.

will produce acceptable level raw observations. The selection of the algorithms is independent of the order.

The structure function $\Phi(\mathbf{x})$ of Figure 4 is given by the expression

$$\begin{aligned}\Phi(\mathbf{x}) = \max\big(&\min(x_{1,1}, x_{1,2}, x_{1,3}, x_{1,4}, x_{1,5}),\\ &\min(x_{1,1}, x_{1,2}, x_{1,3}, x_{1,4}, x_{1,6}), \ldots,\\ &\min(x_{1,6}, x_{1,7}, x_{1,8}, x_{1,9}, x_{1,10})\big).\end{aligned} \tag{15}$$

Assuming that the individual algorithms are independent with equal probability $p(t)$, then the reliability of software component is

$$p_s(t) = P(\mathbf{y}(t) \geq 5) = \sum_{x=5}^{10} \binom{10}{x} p^x (1-p)^{(10-x)}. \tag{16}$$

Due to the fact that $\mathbf{y}(t) \sim \text{binom}(n, p(t))$. The block diagram of the $x_{N,1,10}$ is given by Figure 5.

The corresponding reliability reads

$$\begin{aligned}&p_{N,1,10}\\ &= (p_{N,10,1} + p_{N,10,2} + p_{N,10,3})\\ &\quad - (p_{N,10,1}p_{N,10,2} + p_{N,10,1}p_{1,10,3} + p_{N,10,2}p_{N,10,3})\\ &\quad + p_{N,10,1}p_{N,10,2}p_{N,10,3}.\end{aligned} \tag{17}$$

Hardware Component of Module $M_{N,1}$. The qualities of the GNSS receiver, firmware robustness, GNSS antenna, and choke ring quantify the hardware component. Figure 6 shows the block diagram of the hardware component of the network module $M_{N,1}$.

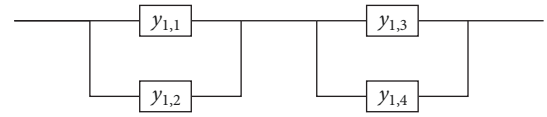

Figure 6: Block diagram of hardware component of module $M_{N,1}$. The left block describes the GNSS receiver and the right is for the GNSS antenna.

The elements of the hardware component of the network module $M_{N,1}$ are as follows:

(i) Let $y_{1,1}$ denote the GNSS receiver type.

(ii) Let $y_{1,2}$ denote the rover software known as firmware to decode the GNSS signals.

(iii) Let $y_{1,3}$ denote the GNSS antenna type.

(iv) Let $y_{1,4}$ denote the choke ring that allows better reception of low elevation angle GPS satellites and improved multipath rejection.

(v) Let $y_{1,5}$ denote duplicated system (as discussed in the next section).

The structure function $\Phi(\mathbf{y})$ is given by the expression

$$\begin{aligned}\Phi(\mathbf{y}) &= \min(\max(y_{1,1}, y_{1,2}), \max(y_{1,3}, y_{1,4}))\\ &= (y_{1,1} \coprod y_{1,2})(y_{1,3} \coprod y_{1,4})\\ &= (y_{1,1} + y_{1,2} - y_{1,1}y_{1,2})(y_{1,3} + y_{1,4} - y_{1,3}y_{1,4}).\end{aligned} \tag{18}$$

The reliability of the hardware of the module $M_{N,1}$ reads

$$\begin{aligned}&p_s(t)\\ &= (p_{1,1} + p_{1,2} - p_{1,1}p_{1,2})(p_{1,3} + p_{1,4} - p_{1,3}p_{1,4}).\end{aligned} \tag{19}$$

Hardware Component Improvement. In order to ensure continuous raw data delivery at the station, duplicated hardware components are recommended. This task is accomplished by a parallel coupling of the module $M_{N,1}$, defined by Figure 6. Applying the definition of reliability computation of parallel coupling (Equation (C.2)), the duplicated HWC reliability reads

$$p(t) = p_s(t) + p_s(t) - [p_s(t)]^2 = p_s(t)[2 - p_s(t)], \tag{20}$$

where $p_s(t)$ is given by the Equation (19). The drawback of a duplicated system is the financial issues.

3.2.2. Network Ambiguity Resolution. As mentioned in Section 3.1. The key for precise positioning is the correct ambiguity resolution and validation. The module $M_{N,2}$ is composed of two main parts, the first part is the ambiguity processing algorithms performance, and the second part is the statistical ambiguity quality indicators derived from the processing chain of the ambiguity.

The components of the module $M_{N,2}$ are as follows:

(i) Let $x_{2,1}$ denote the float solution of the ambiguity obtained via least square or Kalman filter.

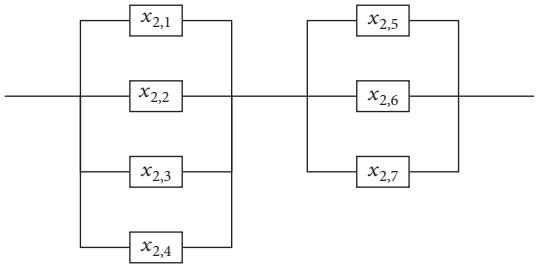

Figure 7: Network ambiguity resolution module $M_{N,2}$. The first block of this figure represents the ambiguity processing algorithms and the second block is the ambiguity quality indicators.

(ii) Let $x_{2,2}$ denote the LAMBDA method [29] applied to a float solution to reduce the search space and to obtain a fix solution.

(iii) Let $x_{2,3}$ denote the validation procedures to validate the final solution.

(iv) Let $x_{2,4}$ denote the administration of the ambiguities.

(v) Let $x_{2,5}$ denote the success rate of the ambiguities resolution.

(vi) Let $x_{2,6}$ denote the ambiguity dilution of precision (ADOP) [30]. ADOP measures the precision of the ambiguities and can be viewed as a quality indicator.

(vii) Let $x_{2,7}$ denote time to fix.

The block diagram of the $M_{N,2}$ is given by Figure 7.

Structure Function of $M_{N,2}$. The structure function of the module $M_{N,2}$ reads

$$\begin{aligned}\Phi(\mathbf{x}) &= \min\left(\max\left(\Phi_1(x)\right), \max\left(\Phi_2(x)\right)\right)\\ &= \min\left(\max\left(x_{2,1}, x_{2,2}, x_{2,3}, x_{2,4}\right),\right.\\ &\left.\max\left(x_{2,5}, x_{2,6}, x_{2,7}\right)\right) = 1 - \left[\prod_{i=1}^{4}\left(1 - x_{2,i}\right)\right]\left[1\right.\\ &\left. - \prod_{i=5}^{7}\left(1 - x_{2,i}\right)\right].\end{aligned} \tag{21}$$

Reliability of $M_{N,2}$. Reliability of the module $M_{N,2}$ reads

$$\begin{aligned}p_s(t) &= \left\{1 - \prod_{i=1}^{4}\left(1 - p_{2,i}\right)\right\}\left\{1 - \prod_{i=5}^{7}\left(1 - p_{2,i}\right)\right\}\\ &= \min\left(P_1, P_2\right) = P_1 P_2\end{aligned} \tag{22}$$

Figure 8: Block diagram of network correction quality module $M_{N,3}$.

dropping the index 2 in the expression of $p_s(t)$ and compute P_1 and P_2

$$\begin{aligned}P_1(t) &= \sum_{i=1}^{4} p_i - \prod_{i=1}^{4} p_i\\ &\quad - \left\{p_1p_2 + p_1p_3 + p_1p_4 + p_2p_3 + p_2p_4 + p_3p_4\right\}\\ &\quad + \left\{p_1p_2p_3 + p_1p_2p_4 + p_1p_3p_4 + p_2p_3p_4\right\},\\ P_2(t) &= \sum_{i=5}^{7} p_i + \prod_{i=5}^{7} p_i - \left\{p_5p_6 + p_5p_7 + p_6p_7\right\}.\end{aligned} \tag{23}$$

3.2.3. Network Corrections Quality. The quality of the network corrections depends on various parameters, for instance, the estimation algorithms, network status (sparse/dense), the covariance functions, and the smoothing/interpolation algorithms. The components of the module $M_{N,3}$ are as follows:

(i) Let $x_{3,1}$ denote the network reference receivers' separation. Dense network is attractive because the network corrections are better estimated with short distances between reference receivers.

(ii) Let $x_{3,2}$ denote the quality of the estimation algorithm used to estimate the parameter vector $\theta \in \Theta$.

(iii) Let $x_{3,3}$ denote the quality of the covariance function used to model the network correlation errors.

(iv) Let $x_{3,4}$ denote the quality of the interpolation algorithm used to generate the user corrections. Parallel interpolation algorithms will enhance the quality of the user corrections generation and avoid the information loss.

Block Diagram of $M_{N,3}$. The block diagram of the module $M_{N,3}$ is given by Figure 8.

Structure Function of $M_{N,3}$. The structure function of the module $M_{N,3}$ reads

$$\Phi(\mathbf{x}) = \min\left(x_{3,1}, x_{3,2}, x_{3,3}, x_{3,4}\right) = \prod_{i=1}^{4} x_{3,i}. \tag{24}$$

Reliability of $M_{N,3}$. Dropping the index 3, the reliability of $M_{N,3}$ reads

$$p_s(t) = \prod_{i=1}^{4} p_{3,i}. \tag{25}$$

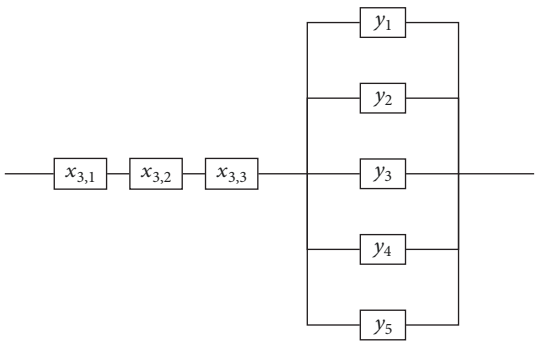

FIGURE 9: Improved block diagram of module $M_{N,3}$. The component $x_{3,4}$ is replaced by a parallel structure function $\phi(y)$.

Amelioration Potential of $M_{N,3}$. Our aim is to provide the user in the field with high quality corrections on an epoch-by-epoch basis. The interpolation/smoothing algorithm plays a central role. We can implement different parallel interpolation/smoothing algorithms that compete about the quality of service parameters. The corrections will be sent from the algorithm with higher score. For more information on this topic, the interested reader is referred to [3].

In this case, replacing the component $x_{3,4}$ with a parallel structure function $\phi(x_{3,4}) = \max(y_1, y_2, \ldots, y_5)$, the computation of the new block diagram is straightforward.

Let q_i denote the functioning probability of unit y_i (Figure 9) for $i = 1, 2, \ldots, 5$. Then the reliability of $x_{3,4}$ reads

$$\begin{aligned} p_{s_{(3,4)}}(t) &= \sum_{i=1}^{5} q_i + \prod_{i=1}^{5} q_i - \{q_1q_2 + q_1p_3 + q_1p_4 + q_1p_5 \\ &+ q_2q_3 + q_2q_4 + q_2q_5 + q_3q_4 + q_3q_5 + q_4q_5\} \\ &+ \{q_1q_2q_3 + q_1q_2q_4 + q_1q_2q_5 + q_2q_3q_4 + q_2q_3q_5 \\ &+ q_3q_4q_5\} - \{q_1q_2q_3q_4 + q_1q_2q_3q_5 + q_2q_3q_4q_5\}. \end{aligned} \tag{26}$$

The improved reliability of module $M_{N,3}$ reads

$$p_s = p_{s_{(3,4)}} \prod_{i=1}^{3} p_{3,i}. \tag{27}$$

3.2.4. Network Data Integrity. The module $M_{N,4}$ responsibility is to carry out the quality control on the corrections field and the corresponding variance-covariance matrices. This includes the following:

(i) Let $x_{4,1}$ denote global test statistics to detect any extremal events that can bias the rover position, corrections field investigation.

(ii) Let $x_{4,2}$ denote the inspection of variance-covariance matrices for Heywood effects algorithm [31].

(iii) Let $x_{4,3}$ denote the application of the imputation algorithm to compute the statistics.

(iv) Let $x_{4,4}$ denote the total variance monitoring algorithm.

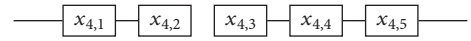

FIGURE 10: Block diagram of module $M_{N,4}$.

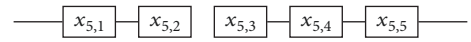

FIGURE 11: Block diagram of module $M_{N,5}$.

(v) Let $x_{4,5}$ denote the generalized variance monitoring algorithm.

Serial coupling is the appropriate choice for the module $M_{N,4}$ and the block diagram is given by Figure 10.

Block Diagram of $M_{N,4}$. See Figure 10.

Structure Function of $M_{N,4}$. The structure function of the module $M_{N,4}$ reads

$$\Phi(\mathbf{x}) = \min(x_{4,1}, x_{4,2}, x_{4,3}, x_{4,4}, x_{4,5}) = \prod_{i=1}^{5} x_{4,i}. \tag{28}$$

Reliability of $M_{N,4}$. Reliability of the module $M_{N,4}$ reads

$$p_s(t) = \prod_{i=1}^{5} p_{4,i}. \tag{29}$$

3.2.5. Network Probability Score. The module $M_{N,5}$ computes the network quality indicators in terms of the successfully ambiguities resolution and the quality of the network corrections. This is the first state vector of the system under investigation.

(i) Let $x_{5,1}$ denote quality indicator for the corrections field.

(ii) Let $x_{5,2}$ denote quality indicator for the uncertainty of corrections field.

(iii) Let $x_{5,3}$ denote quality indicator for the ambiguities expressed by ADOP from Section 3.2.2.

(iv) Let $x_{5,4}$ denote the number of common satellites used in the computation.

(v) Let $x_{5,5}$ denote the number of rejected satellites from computation.

Note that $x_{5,1}$ and $x_{5,2}$ are actually the network RTK quality indicators (RIM, IP, RIU, GBI, and ionospheric status indicator), defined in Section 1.

Serial coupling is the appropriate choice for the module $M_{N,5}$ and the block diagram is represented by Figure 11.

Block Diagram of $M_{N,5}$. See Figure 11.

Structure Function of $M_{N,5}$. The structure function of $M_{N,5}$ reads

$$\Phi(\mathbf{x}) = \min(x_{5,1}, x_{5,2}, x_{5,3}, x_{5,4}, x_{5,5}) = \prod_{i=1}^{5} x_{5,i}. \tag{30}$$

Reliability of Module $M_{N,5}$. The reliability of $M_{1,5}$ reads

$$p_s(t) = \prod_{i=1}^{5} p_{5,i}. \tag{31}$$

3.3. NRTK Baseline Reliability Analysis. This is the second level of the NRTK data processing. The corrections generated by the network are involved to generate the computation point (CP), then the unknown rover coordinates are determined relative to the computation point. This method is known as the relative positioning technique.

Similarity between the baseline and the network data processing exists as we see in the coming subsections.

3.3.1. Rover Receiver Data Integrity. The module $M_{B,1}$ is similar to the module $M_{N,1}$ defined in Section 3.2.1. The quality of the raw observations collected by the rover receiver depends strongly on the statistics methods used to check for anomalies. All variables defined in the module $M_{N,1}$ are applicable to the module $M_{B,1}$.

3.3.2. Baseline Ambiguity Resolution. The module $M_{B,2}$ is similar to the module $M_{N,2}$ defined in Section 3.2.2. All variables defined for the module $M_{N,2}$ are applicable to the module $M_{B,2}$.

3.3.3. Baseline Data Integrity. The module $M_{B,3}$ is similar to the module $M_{N,4}$ defined in Section 3.2.4. All variables defined for the module $M_{N,4}$ are applicable to the module $M_{B,3}$.

3.3.4. Baseline Probability Score. The module $M_{B,4}$ is similar to the module $M_{N,5}$ defined in Section 3.2.5. All variables defined for the module $M_{N,5}$ are applicable to the module $M_{B,4}$.

3.4. NRTK Rover Reliability Analysis. The investigation of the rover position error is the final check. The quality is measured in terms of standard deviations of the topocentric coordinates $(\delta e, \delta n, \delta u)$.

3.4.1. Rover Prediction Function. This module $M_{R,1}$ uses information from the double-difference variance-covariance matrix to compute the prediction of the position error. The number of satellites used in the computation is considered as a parameter.

(i) Let $x_{3,1}$ denote inspection of the main diagonal of variance-covariance matrix.

(ii) Let $x_{3,2}$ denote the total variance monitoring algorithm.

(iii) Let $x_{3,3}$ denote the generalized variance monitoring algorithm.

3.4.2. Rover Position Error. This module $M_{R,2}$ computes the standard deviations of the rover position error $(\delta e, \delta n, \delta u)$ and assigns a final score to determine the state of the rover receiver accuracy.

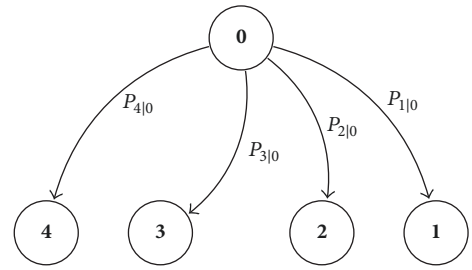

Figure 12: Start state of the rover position accuracy.

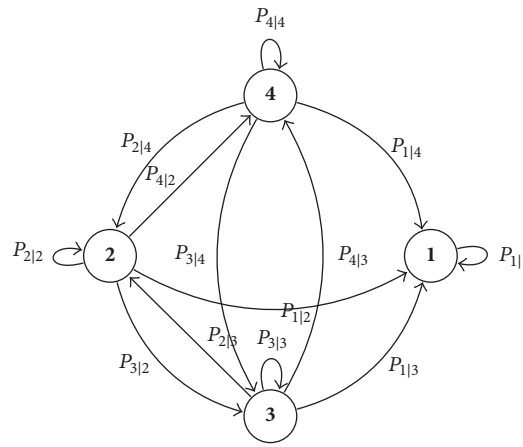

Figure 13: State diagram of the rover position accuracy.

4. Multistate Reliability Analysis

Since the rover position accuracy cannot be represented by a binary system with two performance level states as functioning or failed, the multistate system (MSS) approach is chosen to deal with situations where more than two levels of performance are considered. The material used to construct this section is from Natvig [32].

4.1. Definition of NRTK Performance Levels. Based on the values computed from the score modules $M_{N,5}$ (Section 3.2.5) and $M_{B,4}$ (Section 3.3.4), respectively, a single judging number is assigned to determine the performance level of the rover position accuracy.

The states represent level of performance ranging from the perfect functioning level *perfect* down to the complete failure level *catastrophic*. Five states are defined for a NRTK system, namely, *start*, *perfect*, *acceptable*, *rejected,* and *catastrophic* states.

The rover position accuracy is well described by the state diagrams given by Figures 12 and 13, respectively.

(1) State **4**: perfect functioning level. No complications. The user requirements regarding the position accuracy are satisfied.

(2) State **3**: acceptable position accuracy. Minor complications.

(3) State **2**: rejectable position accuracy. Major complications due to the atmosphere, multipath, or algorithms failure. The user requirements are not satisfied.

(4) State **1**: catastrophic state. The NRTK system is down and not delivering the corrections to the user in the field.

(5) State **0**: start state. The process always starts at this state and can reach any other states.

Note that the states **0**, **4**, **3**, **2** are transient states while the state **1** is absorbing state.

Note that the probabilities $P_{i|j}$ must be computed from real data.

4.2. Penalized Honored Stochastic Averaged Variance. Based on state vectors data, our aim is to construct the NRTK state diagram from the network and baseline. The variance-covariance matrix (VCM) is considered as the state vector and the average variance with respect to the number of observed satellites (n_{sat}) is used to compute the quality indicator on an epoch-by-epoch basis. In addition, the number of rejected satellites (n_{rej}) and the geometry factor (DOP) are used to penalize/honor the average variance.

4.2.1. Penalized Average Variance Component. The total average variance computed from the VCM shall be penalized in case of rejection of satellite(s) with bad data and causes the increase of DOP indicator. The penalized function shall look similar to the following:

(1) Penalized least square (PLS) proposed by Green and Silverman [33, p. 5]

$$S(g) = \sum_{i=1}^{n} \{y_i - g(t_i)\}^2 + \alpha \int_a^b \left\{g''(x)\right\}^2 dx, \tag{32}$$

where y_i is the observations, $g(t_i)$ is the curve we fit to the data, $g''(\cdot)$ is the second derivative of the function $g(\cdot)$, and α is the smoothing parameter and defines the rate of change between the residuals and local variations. Anyway, minimizing $S(g)$ gives the best compromise between smoothness and goodness-of-fit. A large value of α will make the penalty term more in action, while with a small value the first term will be the main contribution.

(2) Information criteria type penalizing the model complexity. Denote by M the model to be investigated and $\dim(M)$ is the length of its parameter vector $\boldsymbol{\theta}$.

Akaike's information criterion (AIC) [34, Chap. 2]

$$\text{AIC}(M) = 2\,\text{log-likelihood}_{\max}(M) - 2\dim(M). \tag{33}$$

The Bayesian information criterion (BIC) of Schwarz (1978) takes the form of a penalized log-likelihood function where the penalty is equal to the logarithm of the sample size times the number of estimated parameters in the model [34, Chap. 3]

$$\begin{aligned}\text{BIC}(M) &= 2\,\text{log-likelihood}_{\max}(M) \\ &\quad - (\log n)\dim(M).\end{aligned} \tag{34}$$

4.2.2. Honored Average Variance Component. Detection and rejection of satellite(s) with bad data are a good thing. The check algorithms shall be honored as long as the DOP values remain in the acceptable region.

The value of the horizontal dilution of precision (HDOP) is expected to be less or equal 2.0, that is, HDOP $\leq$ 2.0.

Forming a new stochastic variable $T_j = \text{HDOP}_j - \mu_{\text{HDOP}}$, then we can monitor the values of T_j over time. Note that μ_{HDOP} corresponds to the mean value of the HDOP in time span Δt.

4.2.3. Balanced Average Variance. Our aim is to put together the pieces defined in Sections 4.2.1 and 4.2.2, respectively, and find a way to balance between the satellite(s) rejection n_{rej} and the HDOP value.

The exponential reweighting algorithm type is an option. The algorithm places more importance to more recent data by discounting older data in an exponential manner. For epoch j, let $k_j = ((n_{\text{obs},j} - n_{\text{rej},j}) - n_{\text{const}})/n_{\text{sys}}$, where $n_{\text{const}} \geq 8$ is the user defined parameter and corresponds to the minimum number of satellites required to compute a reliable solution and preserve a good HDOP value, and $n_{\text{sys}} = 31$ is the total satellites in GPS constellation.

A suitable stabilization factor $\eta \in [0, 1]$ is chosen such that the penalized honored average variance (σ_{phav}) reads

$$\begin{aligned}\sigma_{\text{phasd}}(\eta, k, T) = &\underbrace{\left\{\frac{1}{n_{\text{sat}}}\sum_{i=1}^{n_{\text{sat}}} c_{i,i}\right\}^{1/2}}_{\text{first-term}} \\ &+ \underbrace{\frac{1}{n_j}\sum_{j=1}^{n_j}\left\{\eta k_j + (1-\eta)T_j\right\}}_{\text{second-term}},\end{aligned} \tag{35}$$

where $c_{i,i}$ are diagonal elements of the covariance matrix of the baseline, $n_{\text{obs},j}$ is the number of satellites with valid data used in the computation, $n_{\text{rej},j}$ is the number of rejected satellites by the algorithms, and n_j is the window size which is user defined.

4.2.4. Penalized Honored Average Variance Validation. The parameter vector of (35) is $\boldsymbol{\theta} = (\eta, k, T)$. Our aim is to study the variation of the second term of (35) and try to get some valid answers.

Full details of the penalized honored average standard deviation algorithm are given in Appendix B.

4.3. NRTK Residuals Contribution. NRTK residuals generated by the network and baseline data processing are considered as state vectors and will be to construct the state diagram. The procedure is defined as follows:

(i) choose the time window $\Delta t = 10$ seconds;

(ii) compute the standard deviation of the residuals σ_{res}. Figure 18 shows the concept;

(iii) choose a suitable strategy to map the computed values of σ_{res}.

5. NRTK Reliability Results

The aim of this section is to present the results from the analysis. The level of performance ranging from the perfect functioning level *perfect* down to the complete failure level *catastrophic* shall be determined from the data.

5.1. Horizontal Dilution of Precision (HDOP). The geometry of the visible satellites is considered as an important factor in achieving high quality results especially for point positioning and kinematic surveying. Anyway, the geometry changes with time due to the relative motion of the user and satellites. A measure of the instantaneous geometry is the dilution of precision (DOP) factor.

The DOP values are computed from the variance-covariance matrix in the ECEF coordinate system and converted to the topocentric local coordinate system with its axes along the local north, east, and up (i.e., vertical) by rotational matrix R by applying the law of covariance propagation.

The DOP value can be defined in various ways; PDOP value in the local system is identical to the value in the global system. In addition to the PDOP, two further DOP definitions are used; HDOP, the dilution of precision in the horizontal position, and VDOP, denoting the corresponding value for the vertical component. The interested reader is referred to (Hoffmann-Wellenhof et al., 2008) [1, pp. 262–270]

$$\begin{aligned} \text{GDOP} &= \sqrt{\sigma_e^2 + \sigma_n^2 + \sigma_u^2 + \sigma_t^2}, \\ \text{PDOP} &= \sqrt{\sigma_e^2 + \sigma_n^2 + \sigma_u^2}, \\ \text{HDOP} &= \sqrt{\sigma_e^2 + \sigma_n^2}, \\ \text{VDOP} &= \sqrt{\sigma_u^2}. \end{aligned} \tag{36}$$

Acceptable horizontal DOP value is HDOP $\leq$ 2.0. Figure 14 shows the computed HDOP for the analyzed data set. In addition, Figure 15 shows the viewed satellites. Clearly, the number varies between 8 and 10 satellites.

5.2. Rover Level of Performance Prediction. We will predict the rover level of performance ranging from the perfect functioning level *perfect* down to the complete failure level *catastrophic*. Three classification lines are chosen in order to separate the computed average standard deviations using (35) into four decisions regions based on the values of $\sigma_{\text{pred}} \in \{0.2, .03, .4\}$. Figure 16 shows the concept.

The computation of σ_{pred} using (35) proceeds as follows:

(i) Based on the sliding window size Δt, form a data matrix from the baseline residuals. Compute the variance-covariance matrix VCM_{res} and get and sort in ascending order the diagonal elements D.

(ii) Compute the averaged standard deviation, the first term of (35)

$$\sigma_{\text{avg}} = \left\{ \frac{1}{n_{\text{sat}}} \sum_{i=1}^{n_{\text{sat}}} c_{i,i} \right\}^{1/2}. \tag{37}$$

(iii) Generate a random number $n_{\text{rej}} \in \{0, 1, 2\}$, and compute K_j

$$K_j = \frac{\left(n_{\text{obs},j} - n_{\text{rej},j} - n_{\text{const}}\right)}{n_{\text{tot}}}. \tag{38}$$

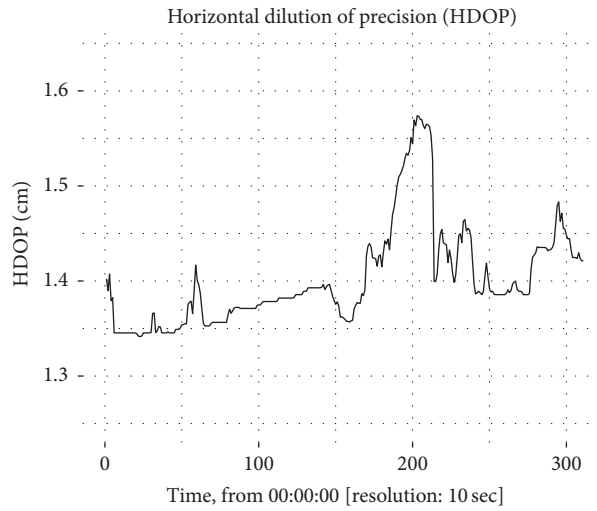

Figure 14: Computed HDOP values. Baseline of ~41 km, year: 2014, DOY: 85.

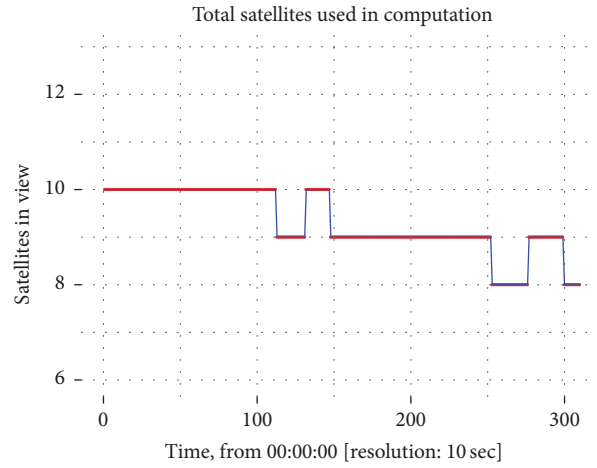

Figure 15: Number of satellites used in the computation. Baseline of ~41 km, year: 2014, DOY: 85. Plotted as red dots connected by blue lines.

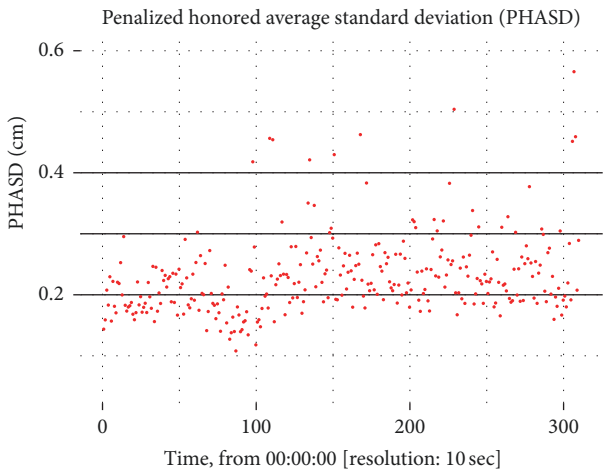

Figure 16: Computed penalized honored average standard deviation. Horizontal lines are used for classification. Baseline of ~41 km, year: 2014, DOY: 85.

(iv) Compute the second term of (35)

$$\sigma_{\text{pen}} = \frac{1}{n_j} \sum_{j=1}^{n_j} \left\{ \eta k_j + (1-\eta) T_j \right\}, \tag{39}$$

where T_j is the HDOP computed from the solution variance-covariance matrix. The computed HDOP values are shown in Figure 14.

6. NRTK Reliability Validation

The aim of this section is to introduce the procedures used to validate the NRTK system reliability. The level of performance ranging from the perfect functioning level *perfect* down to the complete failure level *catastrophic* shall be determined from data.

6.1. NRTK State Diagram Definition. As we mentioned in the introduction, the key of the NRTK method is the measurement of the distance-dependent errors. The variations in the ionospheric and tropospheric fields are assumed constant in a period of time $\Delta t < 10$ s.

Since we have access to the rover position error in the topocentric coordinates system $(\delta_e, \delta_n, \delta_u)$, the state diagram is computed as follows:

(i) Choose the time window $\Delta t = 10$ seconds.

(ii) For each component, compute the standard deviation of the rover position error $\sigma_p = (\sigma_e, \sigma_n, \sigma_u)$. Figure 17 shows the concept.

(iii) Based on the user requirements and the computed values of σ_p, map this value to the performance defined levels, namely, the states $S = \{0, 1, 2, 3, 4\}$.

(iv) Compute transitions probabilities $P_{i|j}$ from data. This task is accomplished by counting the frequencies and computing the associated probability, that is, $p_s = N_s/N_T$, where N_s is the number of times we are visiting the state s and N_T is the total number of events.

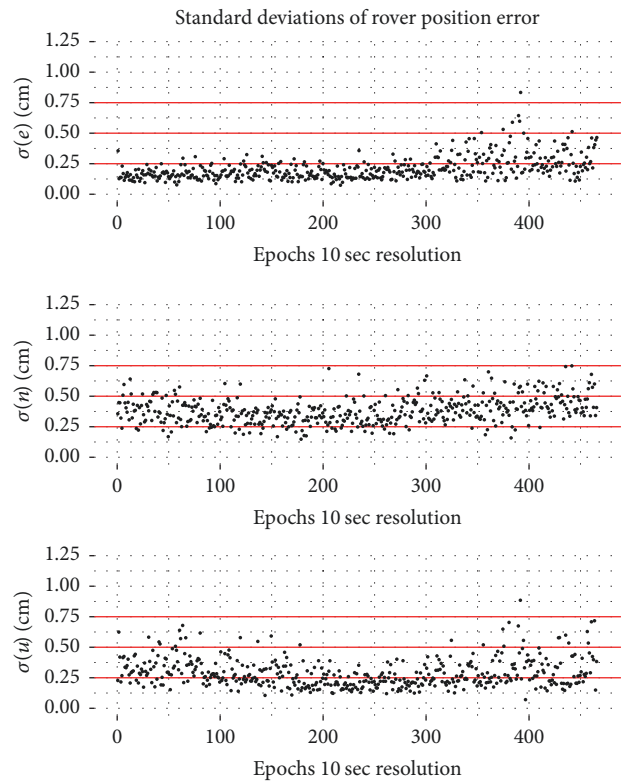

Figure 17: Standard deviations of the rover position errors $(\sigma_e, \sigma_n, \sigma_u)$ in the topocentric coordinate system. Horizontal lines are used for classification. Baseline of ~1 km, year: 2013, DOY: 152.

6.2. States Transition Probabilities. We have computed the transition states probability based on Figure 18, where the threshold T_h values are defined, respectively, $T_h \in \{0.25, .5, .75\}$ cm. Note that $\sum_{j=1}^{4} P_{i,j} = 1$, for $i = 1, \ldots, 4$

$$\begin{array}{c} \\ \text{Next state} \end{array} \begin{array}{c} \text{Current State} \\ \begin{array}{cccc} 4 & 3 & 2 & 1 \end{array} \\ \begin{array}{c} 4 \\ 3 \\ 2 \\ 1 \end{array} \begin{bmatrix} 0.596 & 0.378 & 0.024 & 0.001 \\ 0.234 & 0.668 & 0.098 & 0.001 \\ 0.077 & 0.69 & 0.231 & 0.001 \\ 0 & 0 & 0 & 1 \end{bmatrix} \end{array} = \mathbf{P}. \tag{40}$$

The limiting distribution is obtained by matrix multiplication of the transition matrix:

$$\lim_{n\to\infty} \mathbf{P}_{ij}^{n} = \pi_j, \quad j \geq 0, \tag{41}$$

$$\mathbf{P}^{(50)} = \begin{pmatrix} 0.3312 & 0.5443 & 0.0798 \\ 0.3321 & 0.5459 & 0.0800 \\ 0.3315 & 0.5449 & 0.0799 \end{pmatrix}. \tag{42}$$

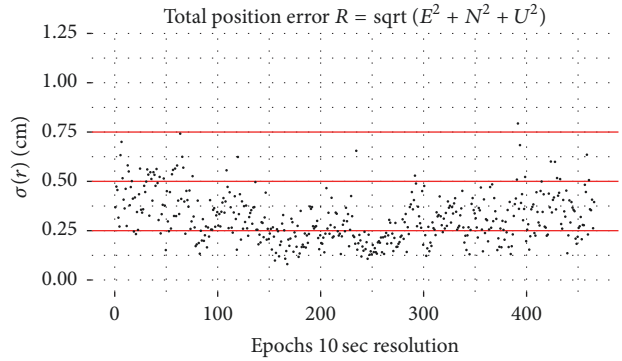

FIGURE 18: Standard deviation of the rover position error. Horizontal lines are threshold values. Baseline of ~1 km, year: 2013, DOY: 152.

We see that each row of $\mathbf{P}^{(50)}$ has almost identical entries; this confirms that (41) converges to some values as $n \to \infty$. It seems that the existence of a limiting probability that the process p will be in state j after a large number of transitions n, and the value is independent of the initial state.

For this data set, the probability of being in state 4 is 33.12%, state 3 is 54.59%, and state 2 is 8.0%.

6.3. State Diagram. Information from the network (Section 3.2) and the baseline (Section 3.3) is combined in such way that a single judging number is mapped to the performance levels with states $S = \{0, 1, 2, 3, 4\}$ and the transitions probabilities $P_{i|j}$ are obtained. This task is accomplished by counting the frequencies and computing the associated probability, that is, $p_s = N_s/N_T$, where N_s is the number of times we are visiting the state s and N_T is the total number of events.

In order to define a single judging number, various schemes are considered, for instance, an averaging scheme or to assign different weights to each component.

7. Discussions and Conclusion

An improvement of the rover position accuracy can be achieved by applying procedures for multistate reliability analysis at the system and user level in NRTK. More concretely, the network corrections, baseline residuals, and the associated variance-covariance matrices are considered as the system states and have a direct influence on the rover position accuracy.

The use of the multistate reliability analysis will help us to get some concrete answers to the following problems

(i) can we trust the corrections provided by NRTK to the user?

(ii) at which level?

(iii) what are the amelioration potentials?

The weaknesses and the strengths of the system have to be identified and the amelioration potential can be achieved by modifying the serial critical components coupling into paralleled one with a cost effectiveness.

The methods tested make it possible to identify the NRTK critical component with bad data so this can be eliminated or downweighted in the positioning process leading to an improvement in the rover position from epoch to epoch.

It is expected that the suggested approach will reduce the number of wrong or inaccurate rover positions encountered by NRTK users in field, which subsequently will lead to a more efficient work flow for NRTK users.

8. Discussions

The rover position accuracy is well described by the state diagram. Based on the values computed by the score modules from the NRTK and the baseline, a single judging number is assigned that determines the performance rate of the rover position accuracy $\rho = (e^2 + n^2 + u^2)^{1/2}$, measured in terms of standard deviations σ_ρ.

The computation of probability of the rover position accuracy in time span $\Delta t = 10$ seconds is carried out as follows:

(1) Network RTK corrections score: based on algorithms efficiency defined in Section 3.2, a probability $p_1 \in [0, 1]$ is assigned to the quality of the corrections.

(2) Baseline score: based on algorithms efficiency defined in Section 3.3, a probability $p_3 \in [0, 1]$ is assigned to the quality of the baseline residuals.

(3) Rover raw observations score: based on algorithms efficiency used to edit the rover raw observations, a probability $p_2 \in [0, 1]$ is assigned to the quality of the rover raw observations.

The validation process is carried out by computing the standard deviations of the rover position error $(\sigma_n, \sigma_e, \sigma_u)$ of topocentric coordinates. A single number, σ_ρ, is assigned and the corresponding state is obtained. Equation (43) shows the mapping used in this investigation

$$F : [0, 1] \times [0, 1] \times [0, 1] \longmapsto [0, 1]$$
$$F(p_1, p_2, p_3) \longmapsto p \in [0, 1] \tag{43}$$

On future work, a monitor station will be used to revalidate our approach for quality control and to carry out classification with

(i) empirical mapping function between the observation and the position domains;

(ii) classification boundaries determination in the observation and position domains.

Appendix

A. Test Data

Data used in this investigation is from the Norwegian RTK network known as CPOS operated by the Norwegian Mapping Authority (NMA). The test area is from the Rogaland region in the south west of Norway. Reference receivers are

Table 1: Subnetwork reference receivers' characteristics.

Site	4-chars ID	Receiver type	Antenna type
Tonstad	TNSC	TRIMBLE NETR9	TRM55971.00
Sirevag	SIRC	TRIMBLE NETR9	TPSCR3_GGD
Stavanger	STAS	TRIMBLE NETR9	TRM55971.00
Akrahamn	AKRC	TRIMBLE NETR9	TPSCR3_GGD
Lysefjorden	LYSC	TRIMBLE NETR9	TRM55971.00
Prestaasen	PREC	TRIMBLE NETR9	TPSCR3_GGD

Table 2: Distances in subnetwork [Km].

Sites	TNSC	SIRC	STAS	AKRC	LYSC	PREC
TNSC	X	56.32	75.00	109.60	44.61	95.23
SIRC	-	X	58.38	91.26	68.50	112.96
STAS	-	-	X	35.83	45.72	64.41
AKRC	-	-	-	X	73.51	65.60
LYSC	-	-	-	-	X	51.45
PREC	-	-	-	-	-	X

Table 3: Reference receiver coordinates, Euref89 *XYZ*.

Sites	*X*	*Y*	*Z*
TNSC	3302221.359	388315.600	5424777.872
SIRC	3323397.670	336993.537	5415277.838
STAS	3275753.912	321110.865	5445041.883
AKRC	3254758.852	295601.453	5458918.670
LYSC	3269684.205	366420.447	5446037.395
PREC	3227088.927	353649.666	5471909.728

equipped with *Trimble NetR9* receivers, tracking GPS, and GLONASS satellite signals. Baselines vary between 35 and 112 km and the height difference between the sites is about 225 m. Tables 1, 2, and 3 give a full description of subnetwork while Figure 19 shows the location of reference receivers. The data used for testing was collected on day of year (doy) 152 in 2013 and doy 85 in 2014, respectively.

B. Penalized Honored Average Standard Deviation

$$\sigma_{\text{phasd}}(\eta, k, T) = \underbrace{\left\{\frac{1}{n_{\text{sat}}}\sum_{i=1}^{n_{\text{sat}}} c_{i,i}\right\}^{1/2}}_{\text{first-term}} + \underbrace{\frac{1}{n_j}\sum_{j=1}^{n_j}\left\{\eta k_j + (1-\eta)\,T_j\right\}}_{\text{second-term}}. \tag{B.1}$$

Algorithm Recipes. The recipes of the algorithm given by (B.1) read as follows:

(1) Compute the effective local coverage (ELC) for epoch j which is defined by the expression: $K_j = (n_{\text{obs},j} - n_{\text{rej},j} - n_{\text{const}})/n_{\text{sys}}$
where

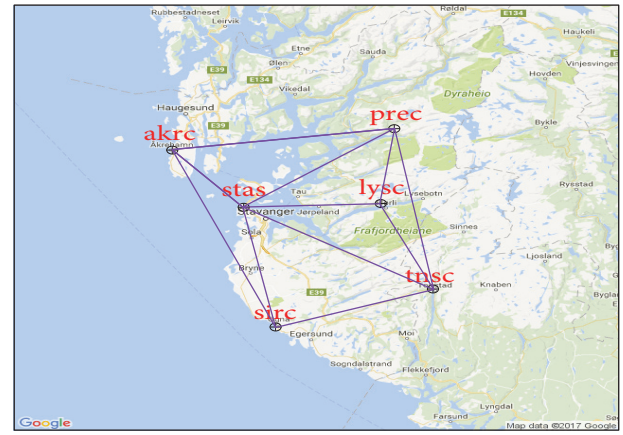

Figure 19: Test area used in this investigation, from Rogaland region. Composed of 6 reference receivers.

(i) $n_{\text{obs},j}$ is total number of satellites used in the estimation process.

(ii) $n_{\text{rej},j}$ is total number of satellites rejected by the algorithms.

(iii) n_{const} is user defined parameter. Default is set to 8.

(iv) n_{sys} is total number of satellites in the GNSS constellation. For the GPS, the value is set to 31.

(2) Position domain quality indicator T_j which is defined as the HDOP

$$T_j = \left\{\sigma_n^2 + \sigma_e^2\right\}_j^{1/2} - \left\{\frac{1}{n_j}\sum_{i=1}^{n_j}\left(\sigma_{n,i}^2 + \sigma_{e,i}^2\right)\right\}^{1/2} = \text{HDOP}_j - \mu_{\text{HDOP}}. \tag{B.2}$$

(3) Stabilization factor η combines and balances between T_j and K_j. A reasonable combination is to binomial/exponential trial:

$$\frac{1}{n_j}\sum_{j_1}^{n_j}\left(\eta k_j + (1-\eta)\,T_j\right), \tag{B.3}$$

where n_j is the window size and is user defined. Default is set to 10.

(4) Operation level: the second term in (B.1) shall operate on the same level as the first term and shall have the same unit. This is accomplished by adjustment of parameters η, K_j, and T_j.

(5) Stabilization factor η can be implemented by the Danish method.

C. Reliability Computation Technique

In this section we present how the computation of the reliability of parallel structure is carried out step by step.

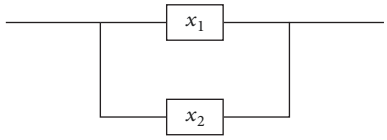

Figure 20: Block diagram of two parallel components.

C.1. Block Diagram. See Figure 20.

C.2. Structure Function. The structure function $\Phi(\mathbf{x})$ of the Figure 20 reads

$$\Phi(\mathbf{x}) = \max(x_1, x_2) = x_1 + x_2 - x_1 x_2. \quad \text{(C.1)}$$

The corresponding reliability reads

$$R(\Phi(x)) = p_1 + p_2 - p_1 p_2. \quad \text{(C.2)}$$

In case of more than two components, the computation of the reliability function $R(\Phi(x))$ is straightforward. The first step is to divide the whole system components into two main components and applying the formula given by (C.2). The next step is to substitute each individual reliability function with the corresponding terms. The last step is simple calculations.

Conflicts of Interest

The authors declare that there are no conflicts of interest regarding the publication of this paper.

Acknowledgments

The international GNSS Service (IGS) is acknowledged for providing geodetic infrastructure and geodetic products used in this work. The authors would also like to thank Jon G. Gjevestad for proofreading of this paper.

References

[1] B. Hofmann-Wellenhof, H. Lichtenegger, and E. Wasle, *GNSS—Global Navigation Satellite Systems: GPS, GLONASS, Galileo, and More*, Springer, Vienna, Austria, 2008.

[2] A. Leick, *GPS Satellite Surveying*, John Wiley & Sons, 2015.

[3] M. Ouassou, A. B. O. Jensen, J. G. O. Gjevestad, and O. Kristiansen, "Next generation network real-time kinematic interpolation segment to improve the user accuracy," *International Journal of Navigation and Observation*, vol. 2015, Article ID 346498, 15 pages, 2015.

[4] H. J. Euler, C. R. Keenan, B. E. Zebhauser, and G. Wübbena, "Study of a simplified approach in utilizing information from permanent reference station arrays," in *Proceedings of the National Technical Meeting of the Satellite Division of the Institute of Navigation (ION GPS '01)*, vol. 104, pp. 371–391, 2001.

[5] F. Takac and O. Zelzer, "The relationship between network RTK solutions MAC, VRS, PRS, FKP and i-MAX," in *Proceedings of the 21st International Technical Meeting of the Satellite Division of the Institute of Navigation (ION GNSS '08)*, pp. 348–355, September 2008.

[6] H. Landau, U. Vollath, and X. Chen, "Virtual reference station systems," *Journal of Global Positioning Systems*, vol. 1, no. 2, pp. 137–143, 2002.

[7] G. Wuebbena, A. Bagge, G. Seeber, V. Boeder, and P. Hankemeier, "Reducing distance dependent errors for real-time precise DGPS applications by establishing reference station networks," in *Proceedings of the 9th International Technical Meeting of the Satellite Division of the Institute of Navigation (ION GPS '96)*, vol. 9, pp. 1845–1852, September 1996.

[8] J. Raquet and G. Lachapelle, "Development and testing of a kinematic carrier-phase ambiguity resolution method using a reference receiver network," *Navigation*, vol. 46, no. 4, pp. 283–295, 1999.

[9] J. F. Raquet, "Development of a method for kinematic GPS carrier-phase ambiguity resolution using multiple reference receivers," UCGE Reports Number 20116, 1998.

[10] J. Xue and K. Yang, "Dynamic reliability analysis of coherent multistate systems," *IEEE Transactions on Reliability*, vol. 44, no. 4, pp. 683–688, 1995.

[11] Y. Gu and J. Li, "Multi-state system reliability: a new and systematic review," *Procedia Engineering*, vol. 29, pp. 531–536, 2012.

[12] F. Ohi, *Stochastic Evaluation of Multi-State Coherent Systems*, Omohi College, Nagoya Institute of Technology, Nagoya, Japan, 2012.

[13] M. Hossam-E-Haider, A. Tabassum, R. H. Shihab, and C. M. Hasan, "Comparative analysis of GNSS reliability: GPS, GALILEO and combined GPS-GALILEO," in *Proceedings of the International Conference on Electrical Information and Communication Technology (EICT '13)*, pp. 1–6, IEEE, February 2014.

[14] S. Satyanarayana, D. Borio, and G. Lachapelle, "C/N0 estimation: design criteria and reliability analysis under global navigation satellite system (GNSS) weak signal scenarios," *IET Radar, Sonar & Navigation*, vol. 6, no. 2, pp. 81–89, 2012.

[15] X. Li, M. Ge, X. Dai et al., "Accuracy and reliability of multi-GNSS real-time precise positioning: GPS, GLONASS, BeiDou, and Galileo," *Journal of Geodesy*, vol. 89, no. 6, pp. 607–635, 2015.

[16] A. Angrisano, C. Gioia, S. Gaglione, and G. Del Core, "GNSS reliability testing in signal-degraded scenario," *International Journal of Navigation and Observation*, vol. 2013, Article ID 870365, 12 pages, 2013.

[17] H. Kuusniemi, A. Wieser, G. Lachapelle, and J. Takala, "User-level reliability monitoring in urban personal satellite-navigation," *IEEE Transactions on Aerospace and Electronic Systems*, vol. 43, no. 4, pp. 1305–1318, 2007.

[18] W. Baarda, *A Testing Procedure for Use in Geodetic Networks*, vol. 2, no. 5, Netherlands Geodetic Commission, 1968.

[19] X. Chen, H. Landau, and U. Vollath, "New tools for network RTK integrity monitoring," in *Proceedings of the 16th International Technical Meeting of the Satellite Division of the Institute of Navigation (ION GPS/GNSS '03)*, pp. 1355–1360, Oregon Convention Center, Portland, Oreg, USA, 2003.

[20] L. Wanninger, "Ionospheric disturbance indices for RTK and network RTK positioning," in *Proceedings of the 17th International Technical Meeting of the Satellite Division of the Institute of Navigation (ION GNSS '04)*, pp. 2849–2854, Long Beach Convention Center, Long Beach, Calif, USA, September 2004.

[21] P. Alves, I. Geisler, N. Brown, J. Wirth, and H.-J. Euler, "Introduction of a geometry-based network RTK quality indicator," in *Proceedings of the 18th International Technical Meeting of the*

Satellite Division of the Institute of Navigation (ION GNSS '05), pp. 2552–2563, September 2005.

[22] D. Prochniewicz, R. Szpunar, and J. Walo, "A new study of describing the reliability of GNSS Network RTK positioning with the use of quality indicators," *Measurement Science and Technology*, vol. 28, no. 1, Article ID 015012, 2017.

[23] S. M. Ross, *Introduction to Probability Models*, Academic Press, 8th edition, 2003.

[24] B. Natvig, *Reliability Analysis with Technological Applications*, Department of Mathematics, University of Oslo, 3rd edition, 1998.

[25] A. Hoyland and M. Rausand, *System Reliability Theory: Models, Statistical Methods, and Applications*, vol. 396 of *Wiley Series in Probability and Statistics—Applied Probability and Statistics Section*, Wiley, 2004.

[26] E. Kaplan and C. Hegarty, *Understanding GPS: Principles and Applications*, Artech House Mobile Communications Series, Artech House, 2nd edition, 2005.

[27] G. Xu, *GPS: Theory, Algorithms and Applications*, Springer, Berlin, Germany, 2007.

[28] W. Gurtner and L. Estey, RINEX: The Receiver Independent Exchange Format Version 2.11, 2007.

[29] P. J. Teunissen, P. J. De Jonge, and C. C. J. M. Tiberius, "Performance of the LAMBDA method for fast GPS ambiguity resolution," *Navigation*, vol. 44, no. 3, pp. 373–383, 1997.

[30] D. Odijk and P. J. G. Teunissen, "ADOP in closed form for a hierarchy of multi-frequency single-baseline GNSS models," *Journal of Geodesy*, vol. 82, no. 8, pp. 473–492, 2008.

[31] H. B. Heywood, "On finite sequences of real numbers," *Proceedings of the Royal Society of London Series A*, vol. 134, no. 824, pp. 486–501, 1931.

[32] B. Natvig, *Multistate Systems Reliability Theory with Applications*, Wiley Series in Probability and Statistics, Wiley, 2011.

[33] P. J. Green and B. W. Silverman, *Nonparametric Regression and Generalized Linear Models: A Roughness Penalty Approach*, Chapman & Hall/CRC Monographs on Statistics & Applied Probability, Taylor & Francis, 1993.

[34] G. Claeskens and N. L. Hjort, *Model Selection and Model Averaging*, Cambridge Series in Statistical and Probabilistic Mathematics, Cambridge University Press, Cambridge, UK, 2008.

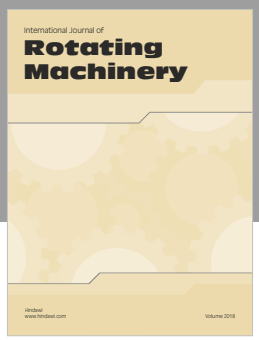

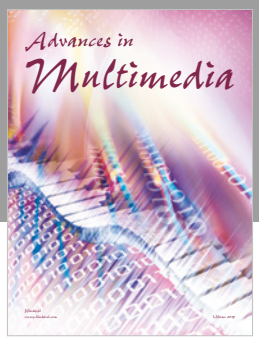

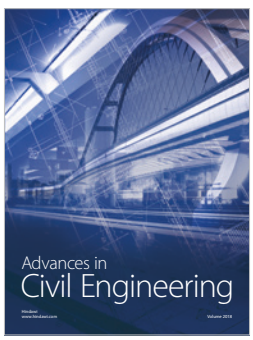

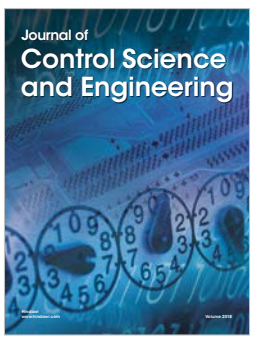

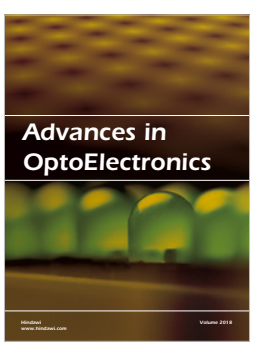

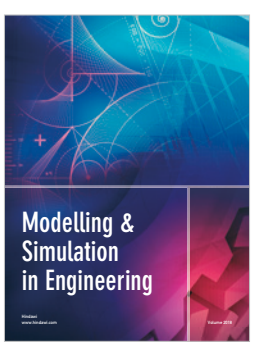

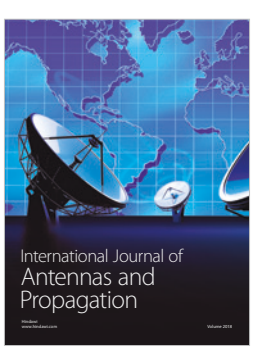

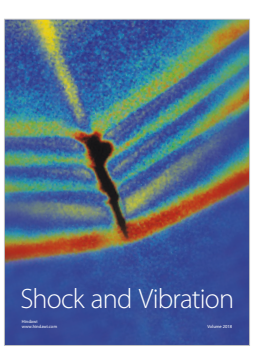

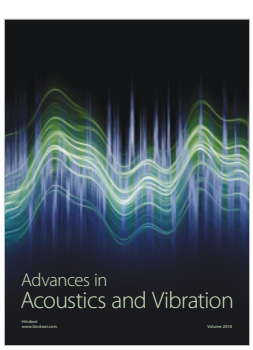

Hindawi

Submit your manuscripts at
www.hindawi.com